The Meteoritical Society

Meteoritics & Planetary Science 42, Nr 11, 2013–2029 (2007)
Abstract available online at http://meteoritics.org

Post-impact structural crater modification due to sediment loading: An overlooked process

Filippos TSIKALAS[†*] and Jan Inge FALEIDE[2]

Department of Geosciences, University of Oslo, P.O. Box 1047 Blindern, NO-0316 Oslo, Norway
[†]Present address: ENI Norge AS, P.O. Box 101 Forus, NO-4064 Stavanger, Norway
[*]Corresponding author. E-mail: filippos.tsikalas@geo.uio.no; filippos.tsikalas@eninorge.com

(Received 02 November 2006; revision accepted 16 February 2007)

Abstract–Post-impact crater morphology and structure modifications due to sediment loading are analyzed in detail and exemplified in five well-preserved impact craters: Mjølnir, Chesapeake Bay, Chicxulub, Montagnais, and Bosumtwi. The analysis demonstrates that the geometry and the structural and stratigraphic relations of post-impact strata provide information about the amplitude, the spatial distribution, and the mode of post-impact deformation. Reconstruction of the original morphology and structure for the Mjølnir, Chicxulub, and Bosumtwi craters demonstrates the long-term subsidence and differential compaction that takes place between the crater and the outside platform region, and laterally within the crater structure. At Mjølnir, the central high developed as a prominent feature during post-impact burial, the height of the peak ring was enhanced, and the cumulative throw on the rim faults was increased. The original Chicxulub crater exhibited considerably less prominent peak-ring and inner-ring/crater-rim features than the present crater. The original relief of the peak ring was on the order of 420–570 m (currently 535–575 m); the relief on the inner ring/crater rim was 300–450 m (currently ~700 m). The original Bosumtwi crater exhibited a central uplift/high whose structural relief increased during burial (current height 101–110 m, in contrast to the original height of 85–110 m), whereas the surrounding western part of the annular trough was subdued more that the eastern part, exhibiting original depths of 43–68 m (currently 46 m) and 49–55 m (currently 50 m), respectively. Furthermore, a quantitative model for the porosity change caused by the Chesapeake Bay impact was developed utilizing the modeled density distribution. The model shows that, compared with the surrounding platform, the porosity increased immediately after impact up to 8.5% in the collapsed and brecciated crater center (currently +6% due to post-impact compaction). In contrast, porosity decreased by 2–3% (currently –3 to –4.5% due to post-impact compaction) in the peak-ring region. The lateral variations in porosity at Chesapeake Bay crater are compatible with similar porosity variations at Mjølnir crater, and are considered to be responsible for the moderate Chesapeake Bay gravity signature (annular low of –8 mGal instead of –15 mGal). The analysis shows that the reconstructions and the long-term alterations due to post-impact burial are closely related to the impact-disturbed target-rock volume and a brecciated region of laterally varying thickness and depth-varying physical properties. The study further shows that several crater morphological and structural parameters are prone to post-impact burial modification and are either exaggerated or subdued during post-impact burial. Preliminary correction factors are established based on the integrated reconstruction and post-impact deformation analysis. The crater morphological and structural parameters, corrected from post-impact loading and modification effects, can be used to better constrain cratering scaling law estimates and impact-related consequences.

INTRODUCTION

Approximately 175 terrestrial impact structures are currently known (e.g., Grieve et al. 1995; Abels et al. 2002; Gersonde et al. 2002; Earth Impact Database 2006). Marine-target impact craters represent ~20% of known craters, a number that is much too low given that more than two-thirds of the Earth's surface is covered by water. This is attributed mainly to plate tectonic destruction processes, sparsity of detailed seismic reflection data from deep-water regions, and the difficulty in

Table 1. Well-preserved and well-studied impact craters that experienced post-impact burial and related modifications.

Crater	Locality	Age (Ma)	Diameter (km)	Target water depth (m)	Maximum post-impact overburden (km)
Chicxulub	Yucatán, Mexico	64.98 ± 0.05	170–310	<50	1–1.5
Chesapeake Bay	Virginia, USA	35.5 ± 0.3	85	200–500	0.5–1
Montagnais	Nova Scotia, Canada	50.5 ± 0.76	45	100–150	1
Mjølnir	Barents Sea, Norway	142 ± 2.6	40	400–600	2–2.5
Bosumtwi	Ghana	1.07	10.5	(exposed)	0.3

identifying buried or exposed submarine craters (e.g., Ormö and Lindström 2000; Dypvik and Jansa 2003). The sparcity of marine craters can be also ascribed to the burial of marine craters by post-impact sediments. Post-impact sediments can reach considerable thicknesses. Although protective at initial stages, extensive burial and associated processes, such as mechanical and chemical compaction and diagenesis may eventually lead to considerable changes in the original crater structure and morphology. Extensive post-impact modifications may obscure many marine impact craters in sedimentary, water-covered targets. The same post-impact processes may result in alterations in typical/expected geophysical signatures at such structures. The post-impact structural and morphological crater modification is, generally, an overlooked process because planetary research of impact structures (where post-impact sediment loading is mostly absent) dominated the impact-related research until recently. In addition, the terrestrial impact record is dominated by crystalline-target impacts on land (e.g., Melosh 1989). Furthermore, post-impact modifications are difficult to quantify if an extensive and dense geophysical dataset of seismic reflection profiles and potential field data is not available, which is usually the case. The impact-induced lateral change in porosity within an impact crater is a key property for understanding impact processes, post-impact compaction, and crater burial history. Although several impact craters have experienced considerable post-impact burial (Table 1), quantification of this process is almost entirely absent from the terrestrial impact record, and therefore a great need exists for such studies.

In this study, post-impact crater structure modifications are examined in detail and exemplified in several well-preserved impact craters such as Mjølnir, Chesapeake Bay, Chicxulub, Montagnais, and Bosumtwi. Direct post-impact effects in geophysical crater response are also quantified, contributing to a better understanding of the post-impact processes and evolution due to sediment loading. This quantification improves the potential for better identification and recognition of marine impact craters on sedimentary targets. The study deals only with imposed effects due to post-impact sediment loading and not other post-impact geological processes, such as long-term tectonism (e.g., Sudbury crater, Milkereit et al. 1994) or hydrothermal alterations (Naumov 2002) that may cause considerable changes in the impact structure or morphology.

POST-IMPACT INFILLING

In marine impacts, post-impact infilling starts with the collapse of the impact-induced water cavity during the modification crater stages (Fig. 1). Collapse of this cavity starts at its base and causes a flow of water and rock debris toward the crater center (e.g., Shuvalov 2002). These processes at marine-target craters may explain the lack of a raised crater rim at the Mjølnir (Tsikalas et al. 1998a, 1998b; Tsikalas and Faleide 2004), Lockne (Sturkell and Lindström 2004), Chesapeake Bay (Poag et al. 1994, 2004), and Chicxulub (e.g., Morgan et al. 2002a) craters, and the beveled crater rim at Montagnais crater (Jansa et al. 1989; Jansa 1993) (cf. Figs. 2 and 3). In marine-impact craters, the impact event leaves a depression on the sea floor into which a considerable amount of sediment is subsequently deposited (Fig. 1).

At Mjølnir (Table 1), continuous sedimentation during the Barremian stage completely buried the impact structure (Fig. 2), and about 1.5–2 km of siliciclastic sediments were subsequently deposited during the Cretaceous-Tertiary period (e.g., Dimakis et al. 1998; Tsikalas et al. 1998a). Late Cenozoic uplift and glacial erosion removed most of the post-impact sediments and sheared the top of the central high (Fig. 2a). Two shallow boreholes, one near the center and another ~30 km from the crater periphery, together with the extensive seismic reflection coverage, provide a detailed chronostratigraphic framework for the post-impact strata at Mjølnir (Tsikalas et al. 2002a). The cross sectional profiles (Fig. 2) reveal that variations in sedimentary thicknesses are influenced by the crater. In particular, most of the post-impact units over the marginal fault zone thicken and sag considerably (Fig. 2b). The discernible thinning of the unit deposited immediately after impact over the peak ring (TD-UB unit of earliest Berriasian-earliest Barremian age; Fig. 2) is evidence for the early existence of the peak ring as a positive feature resulting from the impact. Moreover, the depression around the central high exhibits gradual infilling by progressive accumulation of sediments into the original annular basin, which became completely buried prior to the deposition of the Intra-Barremian unit (IB1-IB2; Fig. 2a). The residual depth of the annular basin at the level of the impact horizon (reflector TD) is ~50 ms (70 m), decreasing to ~35 ms (50 m) at reflector UB (earliest Barremian), whereas the relief is completely smoothed above reflector IB1 (Intra-Barremian). The seismic profiles also indicate onlap against the central high

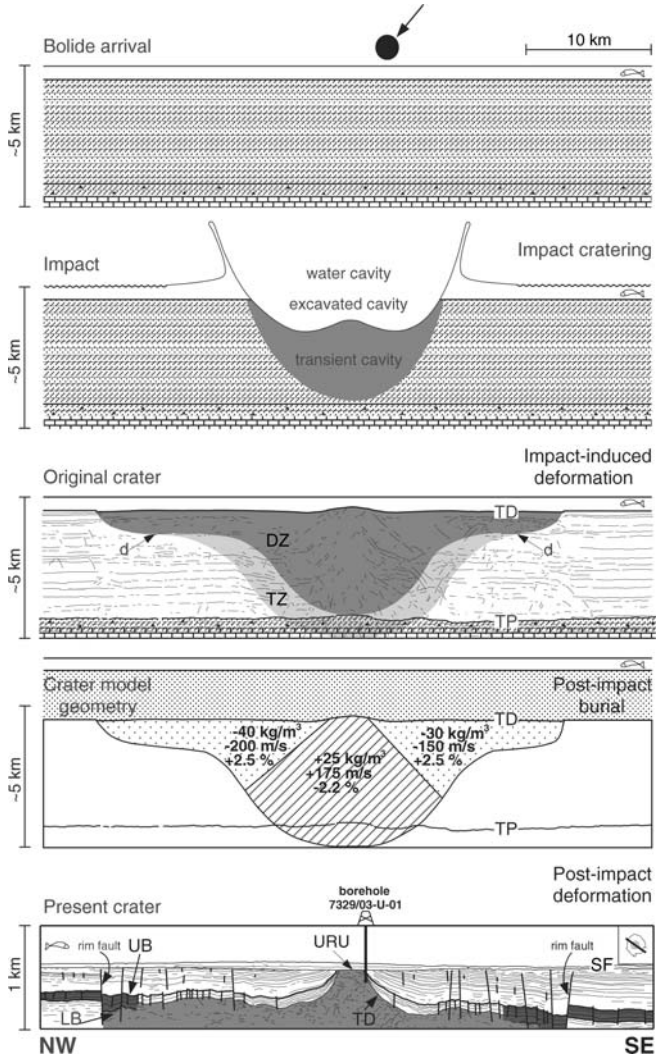

Fig. 1. Schematic cross section showing the Mjølnir impact, resultant radially varying physical property changes, and deformation types. Reflectors UB and LB bound the time of impact (cf. Fig. 2). SF = seafloor; URU = Late Cenozoic upper regional unconformity; UB = lower Barremian; TD = impact horizon (the first continuous reflector above the seismic disturbance); LB = Upper Callovian; TP = top Permian; d = low-angle décollement; DZ = area of intensely disturbed seismic reflections; TZ = transitional area of less disturbance. The crater model geometry (fourth panel) illustrates the modeled impact-produced physical property changes (cf. Fig. 10): modeled density contrasts are given in kg/m^3, seismic velocities in m/s, and porosity anomalies in %.

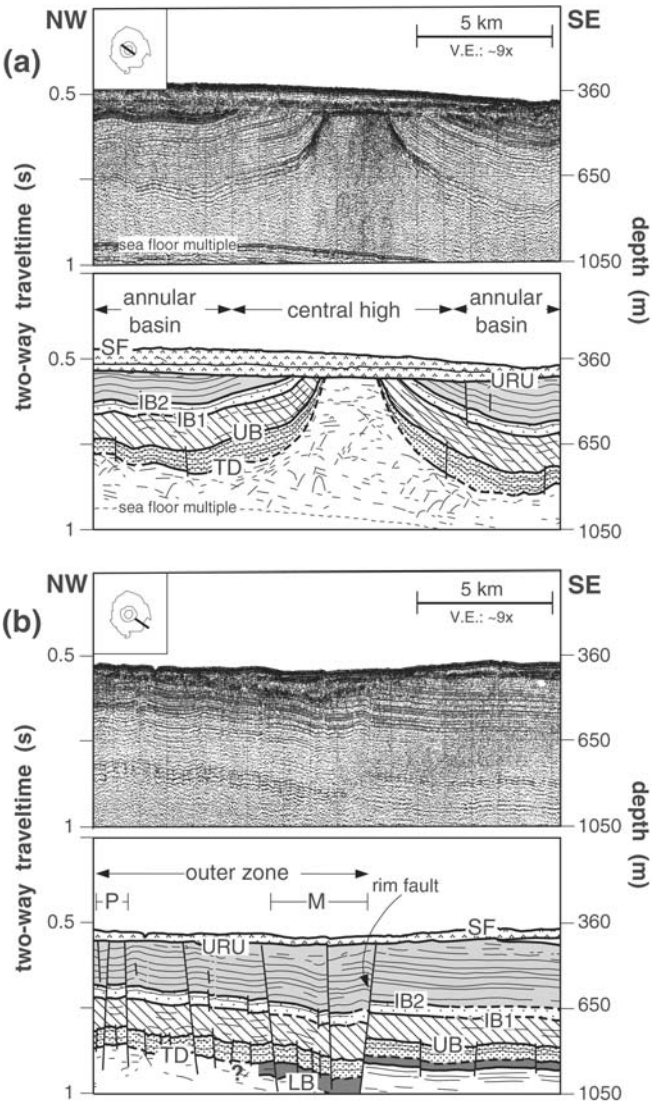

Fig. 2. Mjølnir crater high-resolution single-channel seismic reflection profile examples and interpretations across a) the crater center, and b) across the crater rim. M = marginal fault zone; P = peak ring; IB1 and IB2 = Intra-Barremian reflectors. Other annotations as in Fig. 1.

for most of the early, pre-intra-Barremian (pre-IB1), post-impact sediments. The increase in reflection coefficients between the strata onlapping the central high (Fig. 2a) suggests lateral changes in depositional facies, possibly including turbidite deposits on the steep flanks of the high.

Numerous shallow boreholes in the near vicinity of the Chesapeake Bay crater (Table 1; Fig. 3a) (Poag et al. 2004) and the new USGS-NASA Langley (Horton et al. 2005a, 2005b) and the International Continental Drilling Program (ICDP)-USGS (Gohn et al. 2006) coreholes provide a detailed chronostratigraphic scheme for the siliciclastic post-impact units. There are no precise estimates of the maximum amount of post-impact sediments deposited over the structure. From available seismic reflection profiles (Poag et al. 2004) and utilizing uniform interval velocities of 2–2.5 km/s for the entire post-impact sequence, the maximum post-impact succession is estimated to be ~800 m (ranging from 700–950 m). The impact-related Exmore breccia at Chesapeake Bay crater is overlain by the upper Eocene Chickahominy Formation (Fig. 3a), which is a silty clay unit 60–100 m thick, has distinct thickness variations within the crater, and diminishes in thickness beyond the crater rim (Poag 1996). In addition, sagging and differential subsidence make the Chickahominy Formation mimic the geometry of the underlying Exmore breccia body (Fig. 3a) (Poag et al. 2004). A similar

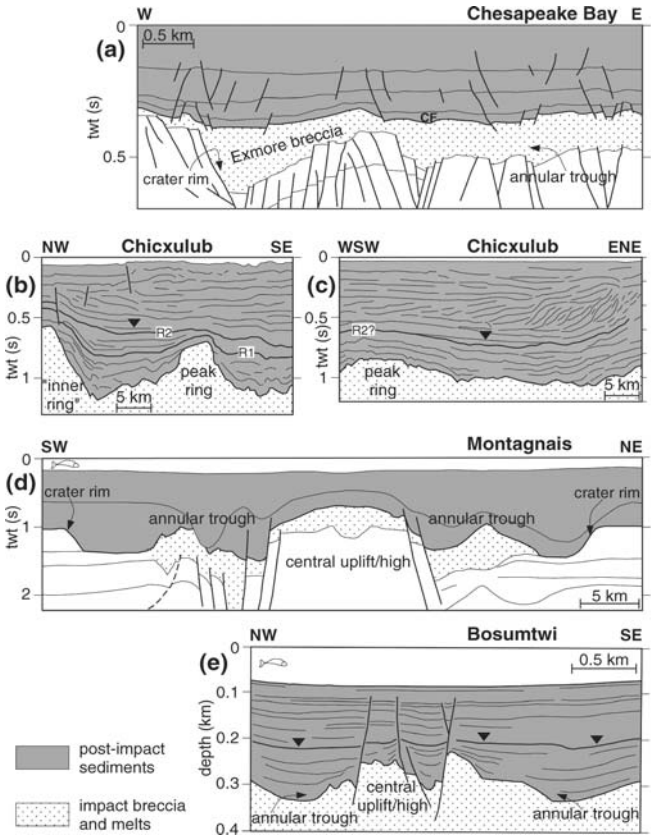

Fig. 3. Interpreted seismic reflection profiles across well-preserved impact craters that experienced post-impact burial and related modifications. a) Chesapeake Bay crater (profile crossing the northwest side of the crater rim [modified from Poag 1996]). CF = Chickahominy Formation. b) Chicxulub crater (re-interpreted part of profile Chicx-B across the northwest side of the crater rim [Snyder and Hobbs 1999b]). For reflectors R1 and R2, see discussion in the text. c) Chicxulub crater (re-interpreted part of profile Chicx-A1 across the northwest side of the crater rim [Snyder and Hobbs 1999b]). d) Montagnais crater (profile across the entire structure [modified from Jansa et al. 1989]). e) Bosumtwi crater (re-interpreted part of profile B2000-1 [Scholz et al. 2002]).

trend is observed at Mjølnir where the TD-UB limestone bed mimics the original crater relief (Fig. 2) (Tsikalas et al. 1998a, 2002b). Furthermore, all post-impact units exhibit discernible depositional and structural thickening and sagging above the Chesapeake Bay structure (Fig. 3a). Similar to the Chickahominy Formation, several Oligocene and lower Miocene post-impact units are considerably thin or absent beyond the crater's rim (Poag 1996; Poag et al. 2004), providing evidence for the persistence of the impact-induced morphological relief for a long time after the Chesapeake Bay physical impact.

The Chicxulub crater (Table 1) is considered a relatively intact and pristine impact crater covered by a thick post-impact Paleogene and Neogene basin filled, in the central crater region, by a thickness of ~1–1.2 s two-way travel time of marine sediments (Figs. 3b and 3c). Several onshore wells and mainly the ~1.5 km deep ICDP Yaxcopoil-1 borehole provide detailed information for the post-impact Cenozoic stratigraphy above the structure (e.g., Kenkmann et al. 2004; Popov et al. 2004). Utilizing seismic velocity information from the seismic reflection and refraction experiments (Brittan et al. 1999; Christeson et al. 1999; Mackenzie et al. 2001; Morgan et al. 2002a, 2002b), a uniform velocity of ~2.5 km/s can be chosen as a representative average for the entire post-impact succession at Chicxulub, and has been used for depth-conversion in our analysis. A variable classification has been used over the years to describe the discernible impact-induced structural ring features within and in the near vicinity of Chicxulub (e.g., Morgan and Warner 1999; Snyder and Hobbs 1999a). However, it seems that a consensus has recently been reached defining a prominent peak ring within the crater, which is bounded by the crater rim, with an outer ring and a weak exterior ring in the crater vicinity (e.g., Morgan et al. 2002b). Figure 3b comprises part of the Chicx-B seismic profile (Snyder and Hobbs 1999b) that does not exhibit exactly the typical dimensions for the structural elements at Chicxulub. The feature in the southeast on Fig. 3b is the peak ring, while the one in the northwest can be part of a more composite peak ring structure, or can be considered as an "inner ring" (Morgan and Warner 1999, their Figs. 4 and 6; Poag et al. 2004, their Fig. 10.25) that is closely related to the crater rim, as it exhibits the largest morphological relief. We chose the latter terminology ("inner ring") as more convenient to differentiate the two prominent elements (Fig. 3b) in our further analysis. Furthermore, the depressions around the prominent peak ring and "inner ring" appear to have filled gradually by progressive accumulation of sediments (Figs. 3b and 3c). In particular, the residual depth of the depression between the two elements at the level of the impact horizon (top of impact breccia; K/T boundary) is 550–600 ms (~700 m), decreasing to 200–250 ms (~300 m) at reflector R1, and 100–125 ms (~150 m) at reflector R2, whereas the relief is almost smoothed stratigraphically farther above (black triangles, Figs. 3b and 3c). The seismic profiles also indicate onlap against the peak ring for most of the pre-R1 post-impact sediments (Figs. 3b and 3c). Reflector R1 represents the first continuous reflector to have surpassed and covered the impact-induced relief, whereas reflector R2 represents the stratigraphic level above which the inherited original impact structure is minimal. Based on interpolation of the onshore Yaxcopoil-1 borehole stratigraphy and seismic profile ties, a preliminary age of ~40 Ma (middle Eocene) was assigned close to reflector R2 (Bell et al. 2004).

At Montagnais crater (Table 1), continuous reflections from post-impact strata of Eocene to Holocene age are observed along seismic reflection profiles tied to the deep-well drilled on the central uplift/high (Jansa et al. 1989; Pilkington et al. 1995), and there is clear evidence of draping of these sequences on the flanks of the central uplift (Fig. 3d). Several periods of submarine current erosion at post-impact

times are also observed, particularly recognizable by the deep channel that cuts into the deposits southwest of the Montagnais central uplift (Fig. 3d) (Jansa et al. 1989). It is believed that the central high/uplift of the structure was a positive relief feature above the seafloor and an obstacle to ocean-bottom currents during post-early Eocene times (e.g., Jansa 1993). This is inferred because the depth of erosional channeling diminishes northward from the center of the structure (Fig. 3d). The central part of the structure is covered by ~0.5 km of post-impact sediments that reach ~1 km in thickness in the annular depressions. The variable thickness of impact breccia is closely connected to both the post-impact erosive undulations and thickness variations of the post-impact strata, indicating prolonged influence of the impact-induced relief and differential sediment loading, especially in the annular depressions surrounding the central high/uplift of the structure (Fig. 3d).

At Bosumtwi crater (Table 1), the post-impact sediments covering the crater structure are 150–300 m thick (Fig. 3e) (Karp et al. 2002; Scholz et al. 2002), and the recent ICDP coring resolved the post-impact stratigraphy (Koeberl et al. 2006). The present-day central uplift/high, with a diameter of 1.9 km and a maximum height of 130 m, was a positive feature immediately after impact as progressive onlap and distinct thickness variations are present within the post-impact sediments (Fig. 3e). Following impact and subsequent sediment accumulation, the impact-induced morphologic relief was diminished (Fig. 3e, black triangles) and progressive accumulation of lacustrine sediments led to post-impact deformation. This is evidenced by the slight sagging of the sequences deposited after complete burial of the original impact relief, and by fault reactivation on the central uplift/high. These faults were likely initiated during collapse of the transient crater (Scholz et al. 2002; Artemieva et al. 2004) and later reactivated due to differential sediment loading and compaction (Fig. 3e).

Several other impact structures are known to have been buried by considerable amounts of post-impact sediments, which potentially could have triggered modifications, but data for a comprehensive analysis do not exist. Such structures include (among others) the Manson (e.g., Hartung and Anderson 1996), Ames (e.g., Carpenter and Carlson 1997), and Lockne (von Dalwigk and Ormö 2001) craters. The Silverpit structure (Stewart and Allen 2002, 2005) is not considered here, as it has not yet been shown to be a genuine impact crater.

Post-impact infilling can complicate seismic interpretation and it may be difficult to differentiate impact-related from post-impact sequences. Seismic profiles with good resolution (Figs. 2 and 3) may help reduce these complications. The depositional influence of the impact-induced relief can take millions of years to diminish depending on the local sedimentation rate and may be followed by complete burial of the crater-related morphology.

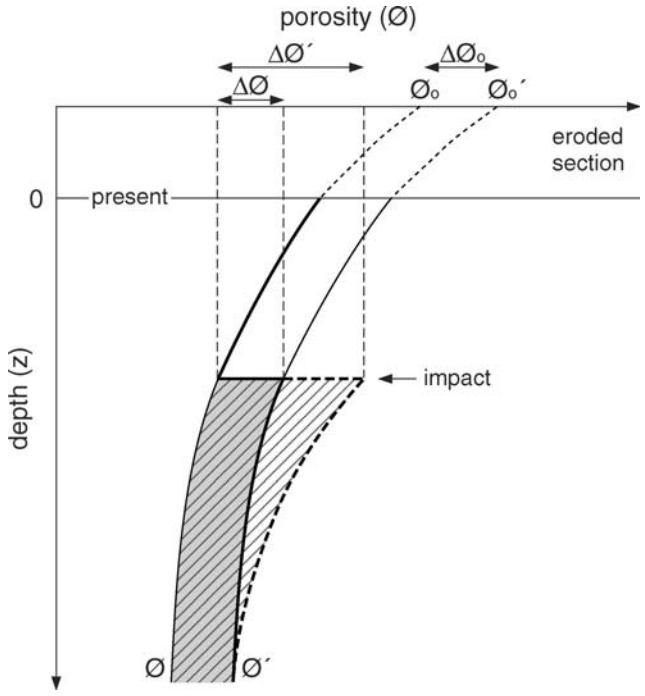

Fig. 4. Generalized porosity-depth functions for sedimentary rocks also incorporating the impact-produced porosity change. Shading denotes a constant porosity anomaly function, whereas hatching denotes an exponentially decreasing function. The various porosities, Ø, are described in the text; $Ø_0'$ is the expected initial/surface porosity of the impact-induced porosity-depth function Ø′, and $Ø_0$ is the porosity anomaly between the initial/surface porosities $Ø_0$ and $Ø_0'$ (modified from Tsikalas et al. 2002a).

In particular, at Mjølnir crater complete burial of the impact-induced morphological relief was completed during Barremian time, i.e., ~15 million years after the impact (Jurassic-Cretaceous boundary, Smelror et al. 2001). Continued deposition subsequently created a substantial overburden. For the Chicxulub crater, Bell et al. (2004) postulated a spatially progressive infilling. In particular, the western and northwestern parts of the Chicxulub post-impact Cenozoic basin were filled ~25 million years after the impact, whereas during a major marine regression a shelf progradation took place in the east ~45 million years after the impact (in Early Miocene). Similarly, at Chesapeake Bay complete burial of the structural crater relief may have required ~15 million years, as lower Miocene units are considerably thin or absent beyond the crater's rim (Poag 1996; Poag et al. 2004).

DIFFERENTIAL VERTICAL MOVEMENTS

During an impact, the propagating shock-pressure waves give rise to extensive in situ fracturing and autochthonous target-rock brecciation (Fig. 1). Impact-induced porosity changes have been identified in damage zones below several craters (e.g., Pilkington and Grieve 1992; O'Keefe et al. 2001) and it is considered that the lateral change in porosity

within an impact structure (especially in a sedimentary target) is a key property in understanding impact processes, post-impact compaction, and crater burial history (Tsikalas et al. 2002a).

Compaction

An exponential reduction function is considered to best approximate the porosity-depth relationship for a compacted sedimentary section (e.g., Wyllie et al. 1956, 1958; Gardner et al. 1974; Sclater and Christie 1980). By introducing an impact-induced porosity change (Fig. 4), the new porosity-depth function, Ø′, which defines the compaction in the crater, becomes:

$$Ø' = Ø_0 e^{-cz} + Ø \quad (1)$$

where $Ø_0$ is the initial porosity, c is the compaction constant, ΔØ is the porosity anomaly induced by the impact, and z is the total overburden (present and eroded). The impact-induced porosity anomaly (ΔØ) can be considered either as constant (retained until present) or as exponentially decreasing ($ΔØ = ΔØ' e^{-cz}$) during burial (Fig. 4).

Seismic reflection profiles across the well-preserved Mjølnir, Cheseapeake Bay, Chicxulub, Montagnais, and Bosumtwi craters (Figs. 2 and 3) clearly reveal post-impact sedimentary thickness variations and lateral facies changes governed by the underlying crater relief. In a generic model for post-impact burial (Fig. 5a), the impact depression is originally filled, and as deposition continues, the crater becomes extensively buried. The progressive loading and the considerable burial trigger structural reactivation and differential compaction (Fig. 5b). In comparison to the undisturbed platform strata (Fig. 5), differential compaction occurs within the crater boundaries due to the existence of both a thick volume of impact-affected and syn-impact rocks together with a thicker post-impact relief-filling unit. Similarly, differential compaction and subsidence occur internally across the crater due to existing lateral thickness variations of the extensively deformed (fractured, brecciated, and structurally elevated) rock volume below the impact horizon (Fig. 1).

Faulting

Analysis of faulting at several craters (Table 1) has shown secondary post-impact phases of faulting in addition to the primary impact-induced phase. Post-impact faulting is closely related to reactivation of major faults generated during impact and initiation of several new faults related to the differential compaction processes (Figs. 2–5).

At Mjølnir crater, detailed structural and stratigraphic analysis shows that the faulting is of varying amplitude and spatial extent, and that there are two major post-impact phases of faulting in addition to the impact-induced phase (Tsikalas et al. 1998a). The impact-induced faulting (LB-TD) is mainly observed within the marginal fault zone; it gave rise to rim faults with throws of ~30–70 ms (45–105 m) (Fig. 2). It is followed by the post-impact Intra Barremian (UB-IB1) and post-Intra Barremian (IB2-URU) phases, separated by a tectonically quiet period during the deposition of unit IB1-IB2 where the surface expression of the crater is buried and disappeared (Fig. 2). Both post-impact phases of faulting at Mjølnir are related to differential vertical movements caused by the development of the thick overburden above the structure (Tsikalas et al. 1998a, 2002b). At Chesapeake Bay crater, differential compaction of the impact-related Exmore breccia is responsible for an extensive number of normal-offset growth faults and fault systems within the post-impact sedimentary succession (Fig. 3a) (e.g., Poag 1996; Poag et al. 2004). The faults mainly cluster in concentric orientations throughout the post-impact strata. The majority of these compaction faults cut through most of the post-impact succession and their throws decrease up-section, indicating that they are growth faults, along which long-term continuous or intermittent movement has taken place (Fig. 3a) (e.g., Poag et al. 2004). At Chicxulub crater, several small-throw faults restricted to the Cenozoic post-impact succession are observed and are mainly concentrated above the “inner ring” and peak ring (Fig. 3b) and the crater rim (e.g., Bell et al. 2004). In detail, the internal post-impact depositional patterns reveal discrete fluxes in relative post-impact vertical movements, with sedimentation initially diminishing the impact-generated relief and subsequent differential compaction creating additional relief that is also filled (black triangles, Figs. 3b and 3c). The latter is possibly accommodated by faulting on top of the prominent structural elements (Fig. 3b). Similarly, at Montagnais crater post-impact reactivation of impact-related faults is observed, mainly at the faults bounding the thick breccia bodies surrounding the central high/uplift (Fig. 3d). At Bosumtwi crater, post-impact fault displacements within the lacustrine section is in the order of 1–3 m, with a maximum offset of 15 m just above the central uplift/high that was prone to reactivation (Fig. 3e) (Scholz et al. 2002).

Reconstruction of the Original Crater Relief

The well-preserved impact structures (Table 1; Figs. 2 and 3) have shown that the distribution and character of the post-impact succession have been influenced initially by the crater structure and morphology, and subsequently by the long-term subsidence of a thick overburden, differential between the un-consolidated impact breccia (autochthonous and allochthonous) inside the crater, and the semi-consolidated or unconsolidated pre-impact sedimentary column outside the crater (Figs. 4 and 5). Therefore, reconstruction of the immediately-after-impact crater relief is of great importance in order to elucidate the post-impact

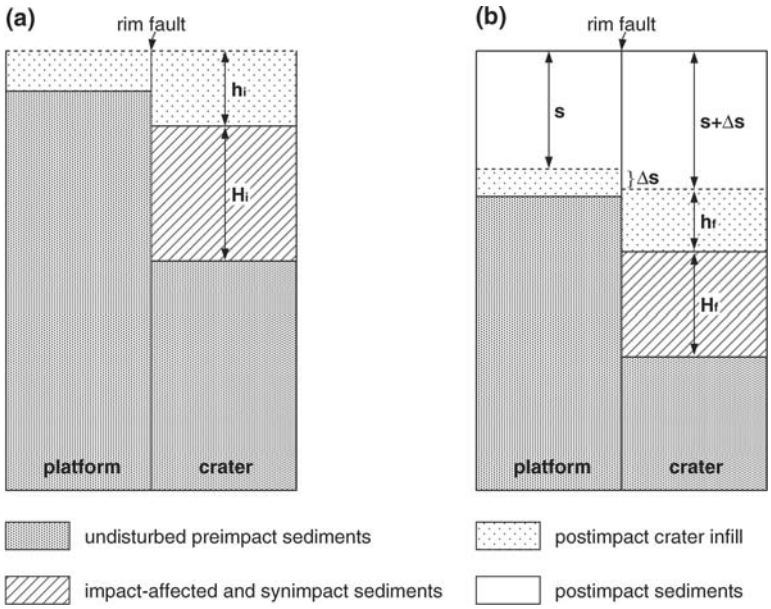

Fig. 5. Schematic diagram of post-impact differential compaction across the crater rim. a) Immediately after the post-impact infilling of the crater, and b) at present. H_i and H_f = initial and present (after post-impact burial) thickness of impact-affected and syn-impact sediments, respectively; h_i and h_f = initial and present (after post-impact burial) thickness of post-impact crater infill, respectively; s = the present and eroded overburden above the infilled crater; Δs = observed differential compaction (modified from Tsikalas et al. 2002a).

evolution, and to provide an original crater relief for volume balance (cratering scaling laws) calculations and comparison with the terrestrial impact record. The approach employed in this study is reconstruction and backstripping of all post-impact sequences in which the deposition has been influenced by the underlying crater relief. Sediment decompaction and fault restoration at time steps, corresponding to post-impact seismo-stratigraphic boundaries, were carried out using the Basin Modelling Toolbox (Fjeldskaar et al. 2004) software for the Mjølnir, Chicxulub, and Bosumtwi craters, which can be considered endmembers in the post-impact burial spectrum receiving an overburden of 2–2.5 km, 1–1.5 km, and 0.3 km, respectively (Table 1). For Mjølnir, we update the results based on the analysis of Tsikalas et al. (1998a), whereas for Chicxulub and Bosumtwi craters, we have conducted an analysis that represents a new aspect of their existing studies.

At Mjølnir (Fig. 6), the depth-conversion was based on the velocity-depth function of Tsikalas et al. (1998b). A well-log derived porosity-depth relationship for siliciclastic sediments ($Ø_o$ ~55%; c 0.42 km^{-1}) developed for the southwestern Barents Sea (Tsikalas 1992) was used to decompact the post-impact sequences. In addition, a uniform Early Cretaceous paleowater-depth of 500 m was incorporated, consistent with the shallow marine depositional environment (Dypvik et al. 1996; Smelror et al. 2001). The Mjølnir crater currently lies beneath ~50–800 m of post-impact sediments (Fig. 6f) (e.g., Tsikalas et al. 1999). Of major importance in the reconstruction analysis is the fact that about 1.5–2 km of siliciclastic sediments were deposited during Cretaceous-Tertiary times (Fig. 6d) (e.g., Dimakis et al. 1998) and were later removed (Fig. 6e) during the Late Cenozoic glacial erosion. Reconstruction suggests that the impact resulted in a very shallow structure with an average crater depth of only ~30 m (Fig. 6a), taken as the depth relative to the pre-impact surface to the top of the allochthonous breccia (reflector TD) (Tsikalas et al. 1998a). Furthermore, the reconstruction dramatically changes the width and height of the central high, as the original crater exhibited a narrower-than-present central high, 4.5–5 km in diameter, that stood ~80 m above the surrounding platform level, in comparison with the present 8 km diameter width and 250 m height (Figs. 6a and 6f). On the other hand, the annular basin was quite prominent with a maximum depth of ~70 m, while the peak ring was not well-developed in the original crater (Figs. 6a and 6f). Furthermore, the reconstruction suggests that on this profile, the original thickness of the allochthonous breccia in the marginal fault zone was ~125–200 m and was reduced by compaction to 75–115 m. Similarly, the original throw on the rim faults when corrected for reactivation and compaction was only 75–105 m, as compared with the cumulative throw of 120–150 m (Tsikalas et al. 1998a). In summary, the decompaction and fault restoration approach at Mjølnir (Fig. 6) demonstrates that the deformation associated with the extensive post-impact overburden considerably enhanced the structural expression of an originally subtle crater and that the present distinct crater expression is largely a post-impact burial phenomenon (Fig. 6) (Tsikalas et al. 1998a).

For Chicxulub crater, the depth-converted section illustrating the peak-ring and “inner-ring” features was used in the reconstruction (Figs. 7a and 8a). The peak ring and “inner

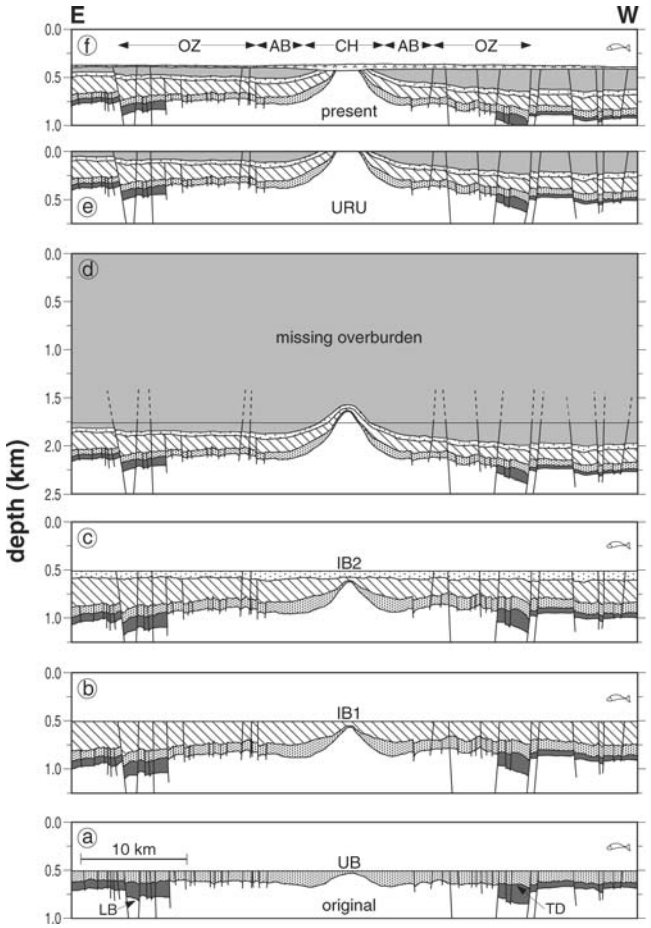

Fig. 6. Reconstruction of the Mjølnir original crater relief along an east-west trending profile by decompaction and fault restoration of the entire post-impact sedimentary succession. Time steps (a–f) correspond to the main unit boundaries. CH = central high; AB = annular basin; OZ = outer zone. Other annotations as in Figs. 1 and 2 (modified from Tsikalas et al. 1998a).

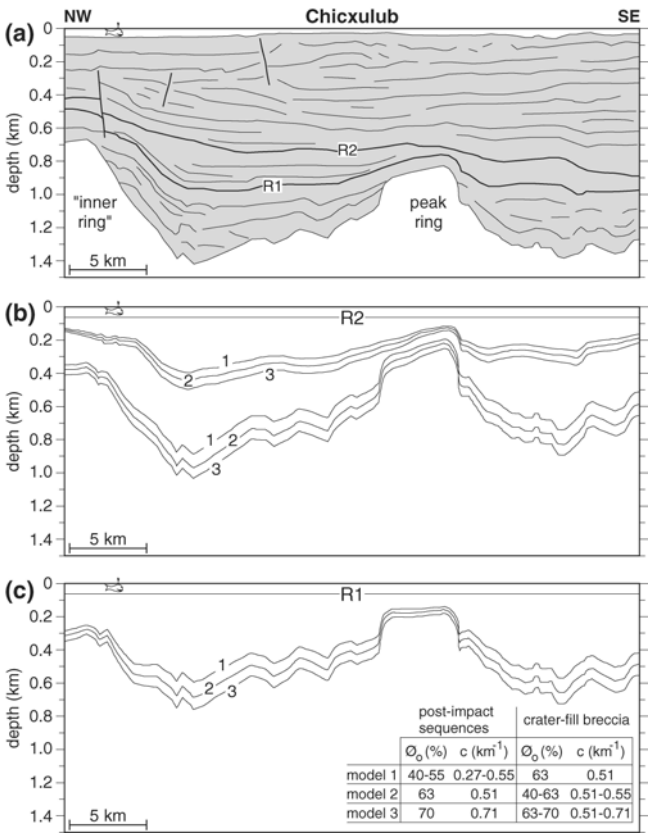

Fig. 7. Reconstruction of the Chicxulub original crater along the a) depth-converted profile in Fig. 3b (re-interpreted part of profile Chicx-B across the northwest side of the crater rim) by backstripping and decompaction utilizing a paleowater depth of 60 m that approximates the current water depth. Reconstruction time steps at reflectors b) R2 and c) R1. A full spectrum of porosity-depth compaction relations of impact and post-impact rocks is incorporated (models 1–3). $Ø_0$ = initial/surface porosity; c = compaction constant. See text for more comprehensive discussion on the reconstructions.

ring" at an average radius of 40 and 60 km from the crater center, respectively, are irregular and rugged (Figs. 3b, 3c, 7a, and 8a). The seismic reflection profiles at Chicxulub show that typically the peak ring is narrow and prominent, ~550 m above the crater floor in Figs. 7a and 8a (400–600 m elsewhere), in the west and northwest, and broader and less prominent (200–300 m above crater floor) to the east and northeast, as in Fig. 3c (e.g., Morgan et al. 1997). Backstripping reconstruction at Chicxulub was employed at two time-steps defined by the sequences bounded by reflectors R2 and R1 in which the deposition has been influenced by the underlying crater relief (Figs. 7 and 8). The Tertiary sediments of the onshore Yaxcopoil-1 borehole are dominated by carbonaceous siltstone to limestone deposits (e.g., Arz et al. 2004; Kenkmann et al. 2004; Popov et al. 2004). Nevertheless, it was argued that the thick offshore post-impact strata may also contain several siliciclastic deposits as revealed from the seismo-stratigraphic depositional patterns, including prominent progradating clinoform buildups (Bell et al. 2004). In order to include various alternative possibilities, numerous porosity-depth relationships ($Ø_0$ and c combinations) ranging between siliciclastic (sand- and shale-dominated alternatives and mixtures), carbonaceous and dolomitic strata were used to decompact the post-impact succession at Chicxulub (Figs. 7 and 8, models 1–3). In addition, two different paleowater depths were used. Initially, a uniform paleowater depth of 60 m (that approximates the current water depth) was used for the backstripped time steps (Figs. 7b and 7c). Finally, a differentiated paleowater depth of 350 m and 100 m was used for the R2 and R1 time steps, respectively (Figs. 8b and 8c), based on the estimates derived from the progradating clinoform geometries (Bell et al. 2004).

Reconstruction at Chicxulub shows that the restored peak ring was not only considerably subdued by comparison with the present configuration, but that the two nearby peak-ring and "inner-ring" structural elements underwent a differentiated post-impact evolution (Figs. 7 and 8). In

particular, the current ~700 m relief of the "inner ring" was originally 300–450 m (Figs. 7 and 8). Similarly, the current ~550 m (range 535–575 m) relief of the peak ring above the surrounding depressions was originally ~500 (range 420–570 m). Note that currently the "inner ring" stands ~150 m above the peak ring (Figs. 7a and 8a), whereas reconstruction shows that immediately after impact this relation was reversed, and the peak ring stood higher by ~100 m (Figs. 7c and 8c). Therefore, there has been a cumulative relative vertical movement of ~250 m between the two prominent structural features. The reconstruction suggests that the post-impact evolution is closely related to the structurally disturbed volume at Chicxulub, containing zones of weakness and a brecciated region of variable thickness at depth (e.g., Christenson et al. 2001; Morgan et al. 2002a). Furthermore, the peak ring lies directly over the inner edge of the collapsed transient cavity and appears to have no consistent gravity or seismic velocity signature (Pilkington et al. 1994; Sharpton et al. 1996; Brittan et al. 1999; Morgan et al. 2000; Christeson et al. 2001). The position of the peak ring above the inner edge of the last slumped blocks is evidence that the peak ring is not vertically uplifted basement material that is emergent through impact breccia (Brittan et al. 1999). The peak ring in Figs. 3b, 7a, and 8a is underlain by a thick volume of crater-fill breccia in comparison to the "inner ring," which is underlain by a smaller volume of impact breccia on top of the inward-slumped blocks (Morgan and Warner 1999, their Figs. 4 and 6; Poag et al. 2004, their Fig. 10.25). The nature and location of both structural elements governed their post-impact differential subsidence behavior, with the peak-ring and its surrounding depressions being prone to greater subsidence in comparison to the "inner ring" (Figs. 7 and 8). Based on isostatic balancing assumptions utilizing the elastic thickness of the crust and time constants for crustal relaxation, Bell et al. (2004) provided subsidence estimates that reveal an original impact-horizon topographic relief in the range of 450–700 m between the crater and the surrounding platform. In Figs. 3b, 7a, and 8a (part of profile Chicx-B; Snyder and Hobbs 1999b), this specific relief corresponds to the relief between the "inner ring"/crater rim and the depression bounding it from the peak ring. Our analysis employing detailed backstripping and decompaction demonstrates that the model of Bell et al. (2004) underestimates the post-impact load effect. The conducted reconstruction (Figs. 7 and 8) provides a robust model for the post-impact structure evolution as it accounts for a broad spectrum of porosity-depth compaction relations between impact-related and post-impact rocks and fits with the impact-induced structures and geometries.

For Bosumtwi crater, we used the depth-converted section in Fig. 3e in the reconstruction analysis. Backstripping and fault restoration was performed at the post-impact stratigraphic level where the impact-induced morphologic relief was diminished (black triangles in Fig. 3e;

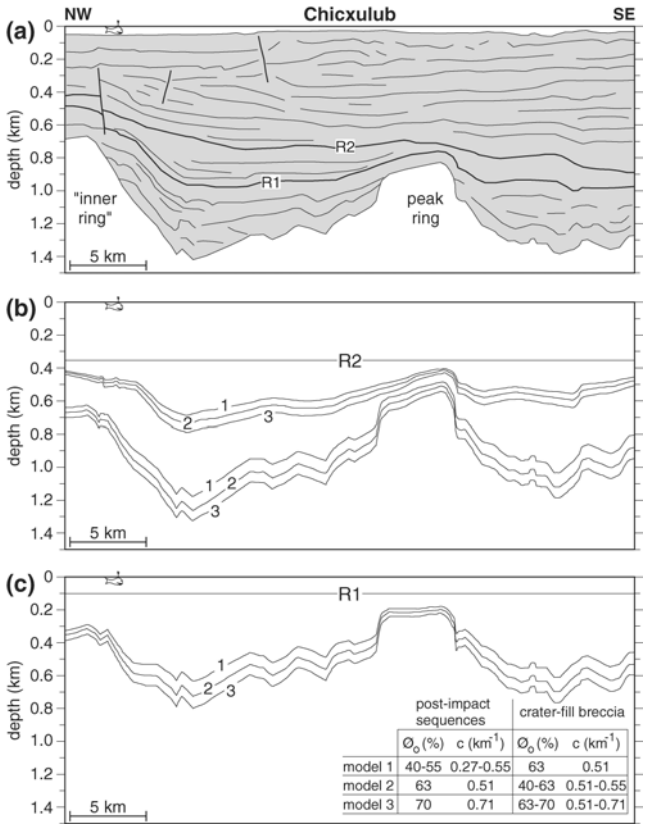

Fig. 8. Reconstruction of the Chicxulub original crater along the a) depth-converted profile in Fig. 3b (re-interpreted part of profile Chicx-B across the northwest side of the crater rim) by backstripping and decompaction utilizing paleowater depths of 350 m and 100 m for reflectors R2 and R1, respectively. Reconstruction time steps at reflectors b) R2 and c) R1. A full spectrum of porosity-depth compaction relations of impact and post-impact rocks is incorporated (models 1–3). $Ø_0$ = initial/surface porosity; c = compaction constant. See text for more comprehensive discussion on the reconstructions.

Fig. 9). As at Chicxulub, we used a broad spectrum of porosity-depth relationships ($Ø_0$ and c combinations) to decompact the post-impact succession at Bosumtwi crater (Fig. 9). We used two different uniform paleowater depths: 75 m, which approximates the current water depth (Fig. 9a), and 200 m, used as the maximum possible paleowater depth level (Fig. 9b). Reconstruction at Bosumtwi shows a discernible post-impact evolution for the central uplift/high and the two depressions/annular troughs (western and eastern) surrounding it (Fig. 9). In particular, the current 110 m height (on this particular profile) of the central uplift/high, measured from the base of the western depression, was originally 95 m (range 85–105 m), whereas the current 101 m height of the central uplift/high, measured from the base of the eastern depression, was originally 103 m (range 95–110 m). On the other hand, the current 46 m depth of the western depression (measured from its base up to the relief on its right side) was originally 55 m (range 43–68 m), whereas the current 50 m depth of the eastern depression (measured from

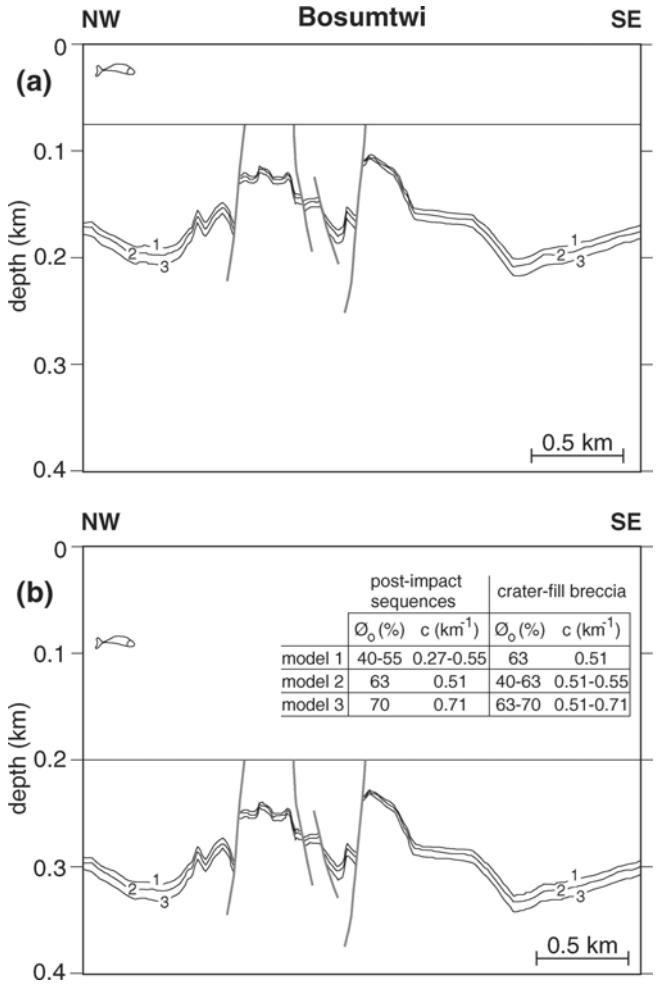

Fig. 9. Reconstruction of the Bosumtwi impact crater along the depth-converted profile in Fig. 3e by backstripping and fault restoration at the post-impact stratigraphic level where the impact-induced morphologic relief was diminished (black triangles in Fig. 3e). a) A uniform paleowater depth of 75 m was utilized. b) A uniform paleowater depth of 200 m was utilized. A full spectrum of porosity-depth compaction relations of impact and post-impact rocks is incorporated (models 1–3). $Ø_0$ = initial/surface porosity; c = compaction constant. See text for more comprehensive discussion of the reconstructions.

its base up to the small terrace on its left side) was originally 52 m (range 49–55 m) (Fig. 9). Recent integrated analysis of gravity and borehole petrophysical data and modeling has shown laterally varying physical properties at Bosumtwi, which are related to impact cratering processes (Ugalde et al. 2005, 2007). Our reconstruction results (Fig. 9) appear to be in accordance with the latter gravity and petrophysics analysis. Similar to the Mjølnir and Chicxulub craters, the post-impact evolution of Bosumtwi crater is closely related to the impact-disturbed target-rock volume and a brecciated region of variable thickness and physical properties at depth. The western part of the reconstructed profile (Fig. 9) compacted relatively more, as it was underlain by a more porous impact breccia unit, whereas the central uplift/high and the eastern depression subsided relatively less, as they were underlain by less porous, melt-rich breccia related to structural uplift (Fig. 9) (Ugalde et al. 2005, 2007).

CHANGES IN GEOPHYSICAL SIGNATURE RESPONSE

A better understanding of crater deformation may be reached by resolving the lateral changes and the interplay between target-rock physical properties (porosity, density, and seismic velocity) during and after impact based on geophysical data and modeling, and numerical modeling of cratering mechanics (e.g., Morgan et al. 2000; Shuvalov et al. 2002; Tsikalas et al. 2002a).

At Mjønir, a quantitative model for the porosity change caused by the impact has been developed using density and seismic traveltime/velocity distributions and post-impact sediment deformation (Fig. 10) (Tsikalas et al. 1998c, 2002a). This model uses well-known equations describing the interrelation between porosity, density, and seismic velocity (Wyllie et al. 1956, 1958; Schlumberger Educational Services 1987, 1989). The model integrates the impact-induced porosity anomaly (Ø) and the corresponding new porosity-depth function (Ø′) (Fig. 4), as well as post-impact differential compaction effects (Fig. 5). The integrated geophysical modeling at Mjølnir demonstrates a close correspondence of geophysical anomalies to the radially varying distribution of structural and morphological units, and to the physical properties distribution. Specifically, the impact resulted in an extensive, 850–1400 km^3 (Tsikalas et al. 1998b), seismically disturbed volume at the impact site (Fig. 10), which exhibits relatively increased porosities and decreased densities and velocities in the highly fractured, brecciated, and collapsed crater periphery. In contrast, the crater center is characterized by decreased porosities and increased densities and velocities, as crater floor rebound and structural uplift processes prevailed (Fig. 10). This setting led to differential subsidence and compaction faulting within the structure, reactivated older faults (especially rim faults), and initiated new ones (Figs. 2, 6, and 10). The extensive post-impact burial (Fig. 6d) led the brecciated periphery to compact more than the denser central crater, resulting in the central high at Mjølnir standing higher than the surrounding platform (Figs. 2, 6, and 10). In comparison to the dramatic impact cratering processes, post-impact burial produced more subtle, long-term alterations which reduced the porosity (and thus density) contrasts between the crater periphery and the platform. According to the compilation of gravity anomalies of impact craters in sedimentary targets by Pilkington and Grieve (1992), a structure of the size of Mjølnir should produce an annular low of about −7 mGal. However, the observed value for Mjølnir is only −1.5 mGal (Fig. 10), though this is still within the range of −1 to −11 mGal determined from a number of craters. Although we recognize

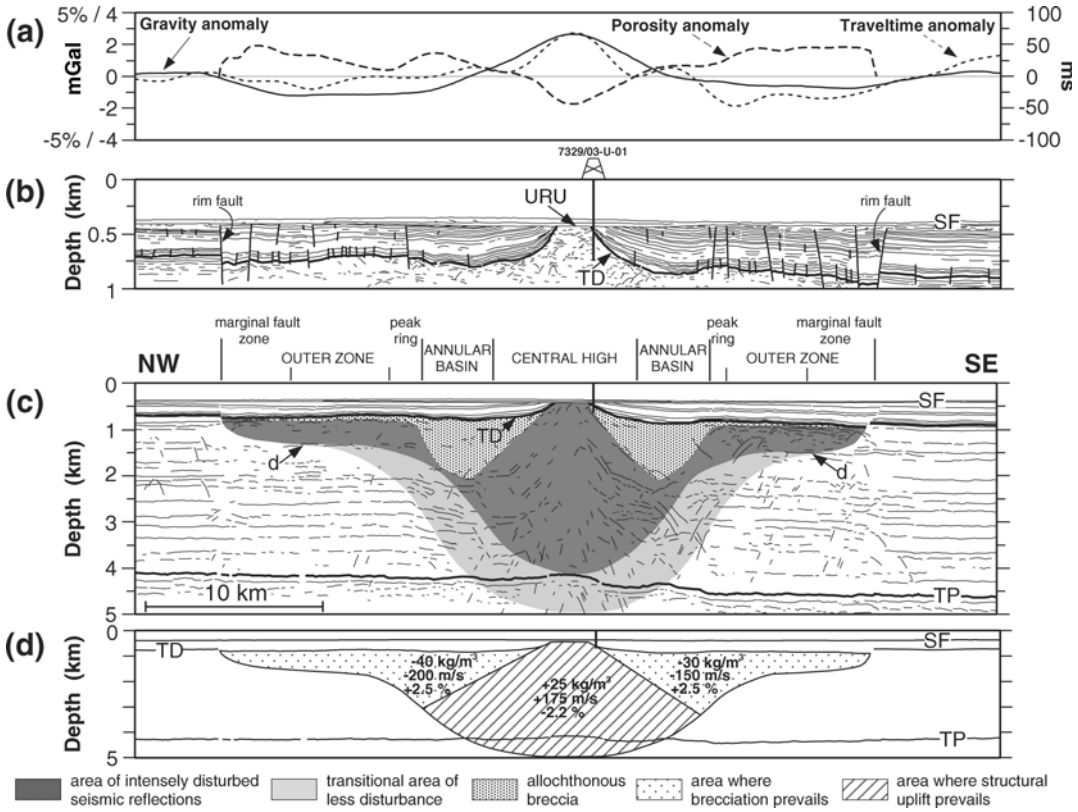

Fig. 10. Geophysical type section along a northwest-southeast trending profile at Mjølnir crater. a) Observed free-air gravity and seismic travel time anomalies and modeled porosity anomaly. b) Interpreted high-resolution single-channel profile. c) Interpreted multi-channel profile (a–c modified from Tsikalas et al. 1998a–c, 2002a). d) Impact crater model with calculated physical property distribution. The crater model geometry in (d) is corrected for regional tilt, and the modeled density contrasts are given in kg/m^3, the seismic velocities in m/s, and the porosity anomalies in %. The type section is representative for the structural and morphological radial zonation of Mjølnir crater. Annotations as in Fig. 1.

that the Mjølnir impact in relatively soft marine sediments may have led to less pervasive brecciation than in continental settings, we conclude that the reduced annular gravity low is also closely connected to the extensive post-impact burial. Therefore, interaction of impact-induced and post-impact processes accounts for the lower-than-expected gravity (and seismic velocity) values, and the corresponding porosity distributions and levels (Fig. 10).

Based on the methodology developed for Mjølnir (Tsikalas et al. 2002a), we have produced a preliminary quantitative model for the porosity changes in the Chesapeake Bay crater (Fig. 11) using the density distributions of Poag et al. (2004; their Fig. 4.37B). Compared with the surrounding sediments, the porosity increased immediately after impact up to 8.5% in the collapsed and brecciated crater center, whereas porosity decreased by 2–3% in the peak ring region. The lateral differentiation of density and porosity, and most probably seismic velocity, is attributed (as at Mjølnir) to the interaction and local spatial prevalence of cratering processes, including brecciation, gravitational collapse, and structural uplift. These processes were responsible for the large seismically disturbed rock volume at the impact site (Figs. 3a and 11). Following impact, the crater was progressively buried by a ~800 m (range of 700–950 m) thick overburden (Table 1), which caused differential compaction of the extensively brecciated central part of the crater fill. This compaction has significantly affected the post-impact crater evolution and decreased the porosity anomaly to values of +6% in the center and −3 to −4.5% in the peak ring region (Fig. 11). A structure of the size of Chesapeake Bay crater should produce an annular gravity low of about −15 mGal (Pilkington and Grieve 1992). Nonetheless, the observed value of −8 mGal (Fig. 11) (e.g., Poag et al. 2004) is still within the −7 to −20 mGal annular gravity anomaly range determined from a number of craters. We recognize that the Chesapeake Bay impact may have been smaller in released energy than its final diameter would indicate based on recent insights from numerical modeling (Collins and Wünnemann 2005). In contrast to Mjølnir, the relatively thin pre-impact sedimentary section at Chesapeake Bay (1–1.5 km; Powars and Bruce 1999; Poag et al. 2004) above crystalline basement would not account for less-pervasive, soft sediment brecciation. Therefore, the moderate Chesapeake Bay gravity signature, in accordance with a similar behavior of the Mjølnir gravity

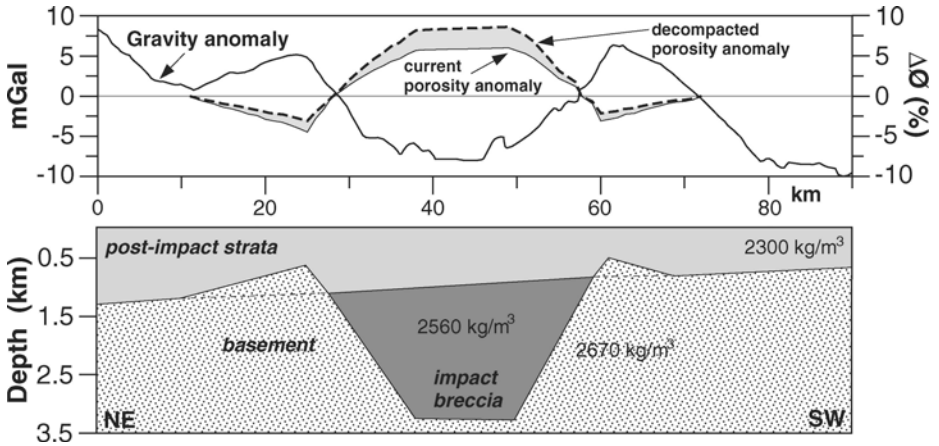

Fig. 11. Simplified Chesapeake Bay crater structure and residual gravity anomaly (modified from Poag et al. 2004), and calculated current and immediately-after-impact porosity anomaly using the modeled density distribution.

response, may be partly ascribed to lesser, long-term alteration due to post-impact burial, which reduced the porosity, and thus density contrasts between the crater structure and the surrounding undisturbed sediments (Fig. 11).

CORRECTION OF CRATER MORPHOLOGICAL AND STRUCTURAL PARAMETERS

Parameters Prone to Post-Impact Burial Modification

The quantitative reconstructions for Mjølnir, Chicxulub, and Bosumtwi craters, together with studies of other craters (Table 1; Fig. 3), demonstrate the great importance of long-term deformation processes operating after impact. As we have shown, the effects of extensive deformation are cumulative and may enhance or subdue the underlying crater morphology (Figs. 2–9), and change the geophysical properties (Figs. 10 and 11).

Peak-ring and inner-ring features are prominent morphological elements in complex impact craters (e.g., Melosh 1989). The peak ring represents the relict transient crater rim uplift, at the location where the transient crater diameter reached its maximum possible extent (Fig. 12a). However, there is no general agreement for the formation mechanism of rings in multi-ring basins and a variety of models have been proposed (e.g., Schultz and Merrill 1981; Melosh 1989; O'Keefe and Ahrens 1999; Grieve and Therriault 2000). At Chicxulub, the peak-ring formation (which is considered crucial in understanding the impact cratering mechanics) is thought to have formed at the region of interaction between upward and outward mass displacement through structural uplift and inwards collapse of the transient cavity (e.g., Morgan et al. 2000). Peak-ring locations in complex craters are used to differentiate the true transient crater diameter (D_t), which differs from the apparent transient crater diameter (D_{at}, referred also as the excavated crater diameter) (Fig. 12a). Utilizing the present-day peak-ring elevation (~550 m height, Fig. 7a), Morgan et al. (1997) estimated the true and apparent transient crater diameters for Chicxulub crater to be ~118 and ~100 km, respectively. These, and other similar estimates, have been incorporated into cratering mechanics analyses, volume balance (cratering scaling laws) estimates, and impact-energy calculations for Chicxulub (e.g., Sharpton et al. 1993, 1996; Hildebrand et al. 1998; Morgan et al. 2000). Our detailed decompaction and backstripping analysis for Chicxulub crater (Figs. 7 and 8) indicates considerably less prominent peak-ring and "inner-ring"/crater-rim features in the original crater morphology. The presence of an originally less prominent peak-ring introduces some interesting geometrical relations that may reduce the estimated extent of both the true and apparent transient crater diameters (Fig. 12). In particular, the fit and height of the paraboloid of resolution (which approximates the form and vertical extent of the transient crater cavity) is quite different when a less prominent peak ring (relict of the transient rim uplift) is introduced (Figs. 12b and 12c). Figure 12 shows that incautious use of the current peak-ring height without any correction for post-impact burial enhancement may lead to overestimation of the true and apparent transient crater diameters.

Impact craters in sedimentary rather than crystalline targets have the advantage that the regular, pre-impact stratification provides reference horizons for correlation and mapping of impact-induced structures (e.g., Morgan and Warner 1999; Tsikalas 2005). At Mjølnir crater, the seismic profiles provide evidence of reflector segments bending upward beneath the central high and the annular basin, indicating elevation of deep strata to shallower levels (Figs. 1 and 10) (Tsikalas et al. 1998b–c; Shuvalov et al. 2002). Based on such geometries, structural uplift was estimated to be 1.0–1.5 km, however, these values are low in comparison with established empirical relations (Tsikalas et al. 1998b). This is because the impacted sediments at Mjølnir have compacted significantly under the load of a maximum post-

impact overburden of 2–2.5 km (Fig. 6) (Tsikalas et al. 1998a). When decompacted, the structural uplift estimates for Mjølnir become ~1.5–2.3 km. These values fit with the predicted structural uplift based on the dimensions of Mjølnir crater and the well-established empirical relations of Pilkington and Grieve (1992) and Cintala and Grieve (1994) that have a best estimate of 2.5 and 2 km, respectively. For Chicxulub crater, seismic velocity models that were used to refine the deep crustal structure indicate a lower limit on the vertical extent of structural uplift of 9 km in the crater center (Christeson et al. 2001). It is reasonable to consider that the ~1–1.5 km post-impact overburden and consequent compaction at Chicxulub considerably reduced any impact-induced porosity excess in the central crater and that this is also reflected in increased densities and seismic velocities in the same area. Therefore, we believe that structural uplift values based on velocity models for Chicxulub are overestimated, as they do not account for the influence of post-impact burial. Both the present-day enhanced peak-ring morphology and structural uplift estimates for Chicxulub have provided direct geophysical values to calibrate numerical modeling of cratering mechanics and released impact energy, which in turn are used to infer the anticipated level of environmental perturbation (Schultz and D'Holdt 1996; Pierazzo et al. 1998; Pierazzo and Melosh 1999; Morgan et al. 2000).

Post-Impact Modification Correction Factor

Several studies (Croft 1985; Melosh 1989, Pilkington and Grieve 1992; Cintala and Grieve 1994; Grieve and Pesonen 1996) have used crater structural and morphological parameters (e.g., estimates of structural uplift, true and apparent transient crater diameters, peak-ring height, rim-height, and annular trough/basin depth) to reveal the cratering processes operating during an impact. The resulting scaling laws are then utilized to average and calibrate other parameters, such as the excavated volume, melt production, and released-energy spectrum. Therefore, overestimation of morphological and structural features that are prone to post-impact burial modification may lead to erroneous conclusions regarding impact-related consequences on a variety of operational scales.

We propose that the establishment of a "post-impact modification correction factor" is prerequisite for several craters. The factor is an estimate of the post-impact morphological and structural changes discussed above, geophysical signature changes, and subdued transient cavity dimensions and structural uplift estimates. Application of the "post-impact modification correction factor" should lead to more accurate estimation of the impact-released energy and, therefore, of related impact consequences. We have made a preliminary attempt to quantify and average the post-impact burial deformation at the five craters discussed herein

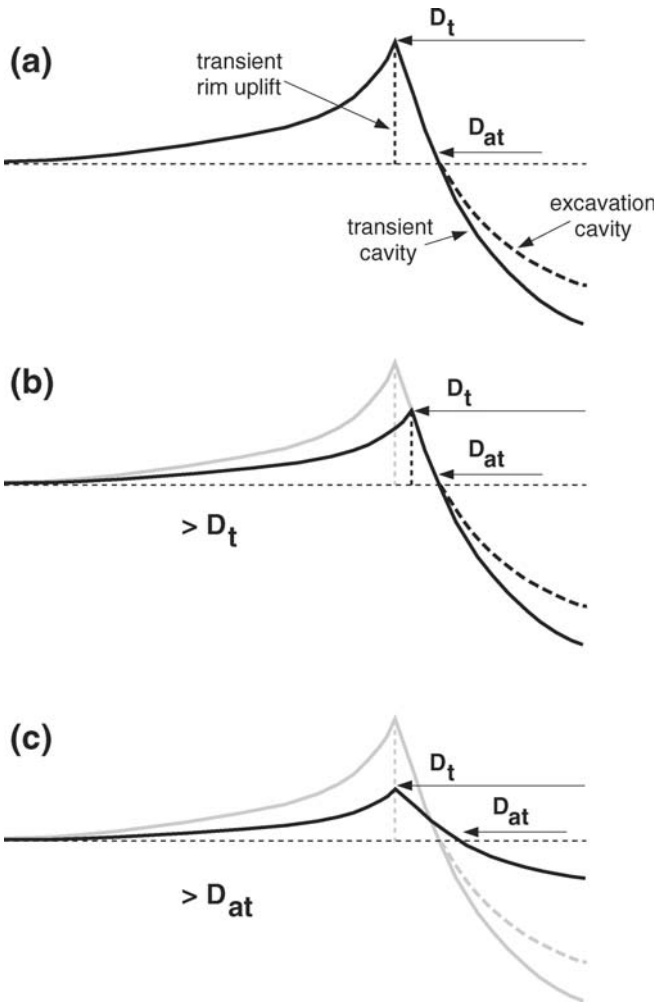

Fig. 12. Schematic diagram of the transient cavity, transient rim uplift, and excavation cavity reconstructions without (a) and with (b), (c) considerations of post-impact burial enhancement and relief exaggeration. D_t = true transient crater diameter; D_{at} = apparent transient crater diameter (referred also as the excavated crater diameter). See text for more detailed description.

(Table 2). Based on our integrated analysis and original crater reconstructions, the post-impact modification correction factors are on the order of 0.35–0.65, 0.25–0.55, 0.25–0.35, 0.10–0.35, and 0.05–0.15 for Mjølnir, Chicxulub, Montagnais, Cheseapeake Bay and Bosumtwi craters, respectively (Table 2). The correction factors (p_f) are indicative of the degree of post-impact burial deformation, and provide a qualitative relation between modification response and overburden thickness, and a quantitative correction of crater morphological and structural parameters utilized in cratering mechanics. These parameters can be corrected as follows:

$$\begin{pmatrix}\text{original crater}\\ \text{morphological/structural}\\ \text{parameter}\end{pmatrix} = \begin{pmatrix}\text{observed}\\ \text{present-day}\\ \text{parameter}\end{pmatrix} \times [1 - p_f] \quad (2)$$

Table 2. Post-impact modification correction factors (p_f) for impact craters that suffered post-impact burial. See text for discussion and proper application.

Crater	Maximum post-impact overburden (km)	Post-impact modification correction factor (p_f)
Mjølnir	2–2.5	0.35–0.65
Chicxulub	1–1.5	0.25–0.55
Montagnais	1	0.25–0.35
Chesapeake Bay	0.5–1	0.10–0.35
Bosumtwi	0.3	0.05–0.15

Existing and future borehole petrophysical data regarding post-impact deposits at Bosumtwi, Chesapeake, and Chicxulub will further constrain the post-impact modification correction factors and their further application to other impact craters.

CONCLUSIONS

We have examined and exemplified post-impact crater morphological and structural modifications caused by sediment loading at five well-preserved impact craters such as Mjølnir, Cheseapeake Bay, Chicxulub, Montagnais, and Bosumtwi. In addition, we reconstructed the original crater morphology for Mjølnir, Chicxulub and Bosumtwi craters by sediment decompaction and fault restoration at time steps that correspond to seismically discernible post-impact unit boundaries. The reconstruction for Mjølnir demonstrates that due to the thick (originally 2–2.5 km, but most of it later eroded) post-impact overburden the central high developed greater prominence, and the peak ring and the cumulative throw on the rim faults were enhanced. Reconstruction of the original Chicxulub crater (1–1.5-km-thick post-impact overburden) indicates that the current ~700-m-relief of the "inner ring"/crater rim and the current 535–575 m relief of the peak ring were originally 300–450 m and 420–570 m, respectively. In addition, a cumulative relative vertical movement of ~250 m took place between the two prominent structural features during post-impact burial. As a result, the peak ring stands higher than the "inner ring"/crater rim in the reconstructed crater. Reconstruction of the original Bosumtwi crater (0.3 km thick post-impact overburden) revealed that the current height of the central uplift/high of 101–110 m contrasts with the original height of 85–110 m. In addition, the depth of the western part of the depression/annular trough was decreased more than the eastern part; original depths were 43–68 m (currently 46 m) and 49–55 m (currently 50 m), respectively.

The reconstructions for the Mjølnir, Chicxulub, and Bosumtwi craters are closely related to the impact disturbed target-rock volume and a brecciated region that varies laterally both in thickness and in physical properties with depth. The lateral changes in physical properties across these impact craters are the result of several counteracting porosity-increasing cratering processes (fracturing, brecciation, and gravitational collapse) and density-increasing ones (crater floor rebound and structural uplift). A new quantitative model for the porosity change produced by the Chesapeake Bay impact uses the modeled density distribution. Compared with the surrounding undisturbed sediments, the porosity increased immediately after impact up to 8.5% in the collapsed and brecciated crater center (currently +6% due to post-impact compaction), whereas porosity decreased by 2–3% (currently −3 to −4.5% due to post-impact compaction) in the peak ring region. The lateral variations in porosity at Chesapeake Bay crater are compatible with similar porosity variation in the Mjølnir crater. Furthermore, the moderate gravity signature in the annular trough at Chesapeake Bay (measured −8 mGal instead of −15 mGal) may be partly ascribed to lesser, long-term alteration due to post-impact burial, decreasing the porosity, and thus, density contrasts between the crater structure and the surrounding sediments.

The study demonstrates the need to establish a "post-impact modification correction factor" for all craters that have experienced post-impact burial. Based on our crater reconstructions and integrated analysis, the post-impact modification correction factors are on the order of 0.35–0.65, 0.25–0.55, 0.25–0.35, 0.10–0.35, and 0.05–0.15 for Mjølnir, Chicxulub, Montagnais, Cheseapeake Bay, and Bosumtwi craters, respectively. The correction factors provide a qualitative measure of modification response to increasing overburden and a quantitative means of correcting crater morphological and structural parameters utilized in cratering mechanics and impact-related consequences at various scales. The study substantiates that post-impact structural and morphological crater modification due to sediment loading, though generally overlooked, is an important process that may subdue or amplify crater features for millions of years following an impact. The improved quantification of the amplitude, spatial distribution, and mode of post-impact deformation and their effects on crater structure and morphology should lead to a better understanding of the mechanics of cratering in sedimentary or two-layer targets.

Acknowledgments–We gratefully acknowledge the Norwegian Defense Research Establishment and the Norwegian Petroleum Directorate for providing the data on the Mjølnir crater. We thank the International Research Institute of Stavanger AS (IRIS) for providing the Basin Modelling Toolbox (BMT) software. We also thank C. W. Poag and B. Milkereit for helpful comments and suggestions

as reviewers, as well as the associate editor J. Ormö for his comments and recommendations. Statoil is acknowledged for the continuous financial support over the last years.

Editorial Handling—Dr. Jens Ormö

REFERENCES

Abels A., Plado J., Pesonen L. J., and Lehtinen M. 2002. The impact cratering record of Fennoscandia—A close look at the database. In *Impacts in Precambrian shields*, edited by Plado J. and Pesonen L. J. Heidelberg: Springer-Verlag. pp. 1–58.

Artemieva N., Karp T., and Milkereit B. 2004. Investigating the Lake Bosumtwi impact structure: Insight from numerical modelling. *Geochemistry, Geophysics, Geosystems* 5:1–20.

Arz J. A., Alegret L., and Arenillas I. 2004. Foraminiferal biostratigraphy and paleoenvironment reconstruction at Yaxcopoil-1 drill hole, Chicxulub crater, Yucatán Peninsula. *Meteoritics & Planetary Science* 39:1009–1111.

Bell C., Morgan J. V., Hampson G. J., and Trudgill B. 2004. Stratigraphic and sedimentological observations from seismic data across the Chicxulub impact basin. *Meteoritics & Planetary Science* 39:1089–1098.

Brittan J., Morgan J. V., Warner M. R., and Marin L. 1999. Near-surface seismic expression of the Chicxulub impact crater. In *Large meteorite impacts and planetary evolution II*, edited by Dressler B. O. and Sharpton V. L. GSA Special Paper #339. Boulder, Colorado: Geological Society of America. pp. 281–290.

Carpenter B. N. and Carlson R. 1997. The Ames meteorite impact crater. *Oklahoma Geological Survey Circular* 100:104–119.

Christeson G. L., Buffler R. T., and Nakamura Y. 1999. Upper crustal structure of the Chicxulub impact crater from wide-angle ocean bottom seismograph data. In *Large meteorite impacts and planetary evolution II*, edited by Dressler B. O. and Sharpton V. L. GSA Special Paper #339. Boulder, Colorado: Geological Society of America. pp. 291–298.

Christeson G. L., Nakamura Y., Buffler R. T., Morgan J. V., and Warner M. 2001. Deep crustal structure of the Chicxulub impact crater. *Journal of Geophysical Research* 106:21,751–21,769.

Cintala M. J. and Grieve R. A. F. 1994. The effects of differential scaling of impact melt and crater dimensions on lunar and terrestrial craters: Some brief examples. In *Large meteorite impacts and planetary evolution*, edited by Dressler B. O., Grieve R. A. F., and Sharpton V. L. GSA Special Paper #293. Boulder, Colorado: Geological Society of America. pp. 51–59.

Collins G. S. and Wünnemann K. 2005. How big was the Chesapeake Bay impact? Insight from numerical modeling. *Geology* 33:925–928.

Croft S. K. 1985. The scaling of complex craters. Proceedings, 15th Lunar and Planetary Science Conference. pp. C828–C842.

Dalwigk I. von and Ormö J. 2001. Formation of resurge gullies at impacts at sea: The Lockne crater, Sweden. *Meteoritics & Planetary Science* 36:359–369.

Dimakis P., Braathen B. I., Faleide J. I., Elverhøi A., and Gudlaugsson S. T. 1998. Cenozoic erosion and the preglacial uplift of the Svalbard-Barents Sea region. *Tectonophysics* 300:311–327.

Dypvik H., Gudlaugsson S. T., Tsikalas F., Attrep M. Jr., Ferrell R. E. Jr., Krinsley D. H., Mørk A., Faleide J. I., and Nagy J. 1996. Mjølnir structure: An impact crater in the Barents Sea. *Geology* 24:779–782.

Dypvik H. and Jansa L. F. 2003. Sedimentary signatures and processes during marine bolide impacts: A review. *Sedimentary Geology* 161:309–337.

Earth Impact Database. 2006. http://www.unb.ca/passc/ImpactDatabase. Accessed November 29, 2007.

Fjeldskaar W., ter Voorde M., Johansen H., Christiansson P., Faleide J. I., and Cloetingh S. A. P. L. 2004. Numerical simulation of rifting in the northern Viking Graben: The mutual effect of modelling parameters. *Tectonophysics* 382:189–212.

Gardner G. H. F., Gardner L. W., and Gregory A. R. 1974. Formation velocity and density—The diagnostic basics for stratigraphic traps. *Geophysics* 39:770–780.

Gersonde R., Deutsch A., Ivanov B. A., and Kyte F. T. 2002. Oceanic impacts—A growing field of fundamental science. *Deep Sea Research Part II*: *Topical Studies in Oceanography* 49:51–957.

Grieve R. A. F., James R., Smit J., and Therriault A. 1995. The record of terrestrial impact cratering. *GSA Today* 5:193–196.

Grieve R. A. F. and Pesonen L. J. 1996. Terrestrial impact craters: Their spatial and temporal distribution and impacting bodies. *Earth, Moon, and Planets* 72:357–376.

Grieve R. A. F. and Therriault A. 2000. Vredefort, Sudbury, Chicxulub: Three of a kind? *Annual Review of Earth and Planetary Sciences* 28:305–338.

Gohn G. S., Koeberl C., Miller K. G., Reimold W. U., Cockell C. S., Horton J. W., Sanford W. E., and Voytek M. A. 2006. Chesapeake Bay impact structure drilled. *Eos* 87:349, 355.

Hartung J. B. and Anderson R. R. 1996. A brief history on investigations of the Manson impact structure. In *The Manson impact structure, Iowa: Anatomy of an impact crater*, edited by Koeberl C. and Anderson R. R. GSA Special Paper #302. Boulder, Colorado: Geological Society of America. pp. 31–43.

Hildebrand A. R., Pilkington M., Ortiz-Aleman C., Chavez R., Urrutia-Fucugauchi J., Connors M., Graniel-Castro E., Camara-Zi A., Halpenny J., and Niehaus D. 1998. Mapping Chicxulub crater structure with gravity and seismic reflection data. In *Meteorites: Flux with time and impact effects*, edited by Grady M. M., Hutchinson R., McCall G. J. H., and Rotherby D. A. Special Publication #140. London: Geological Society of London. pp. 155–176.

Horton J. W. Jr., Powars D. S., and Gohn G. S. 2005a. *Studies of the Chesapeake Bay impact structure—The USGS-NASA Langley corehole, Hampton, Virginia, and related coreholes and geophysical surveys*. USGS Professional Paper #1688. Reston, Virginia: U.S. Geological Survey.

Horton J. W. Jr., Aleinikoff J. N., Kunk M. J., Gohn G. S., Edwards L. E., Self-Trail J. M., Powars D. S., and Izett G. A. 2005b. Recent research on the Chesapeake Bay impact structure, USA—Impact debris and reworked ejecta. In *Large meteorite impacts III*, edited by Kenkmann T., Hörz F., and Deutsch A. GSA Special Paper #384. Boulder, Colorado: Geological Society of America. pp. 147–170.

Jansa L. F., Pe-Piper G., Robertson B. P., and Friedenreich O. 1989. Montagnais: A submarine impact structure on the Scotian Shelf, eastern Canada. *Geological Society of America Bulletin* 101: 450–463.

Jansa L. F. 1993. Cometary impacts into ocean: Their recognition and the threshold constraint for biological extinctions. *Palaeogeography, Palaeoclimatology, Palaeoecology* 104:271–286.

Karp T., Milkereit B., Janle P., Danuor S. K., Pohl J., Berckhemer H., and Scholz C. A. 2002. Seismic investigation of the Lake Bosumtwi impact crater: Preliminary results. *Planetary and Space Science* 50:735–743.

Kenkmann T., Wittmann A., and Scherler D. 2004. Structure and impact indicators of the Cretaceous sequence of the ICDP drill core Yaxcopoil-1, Chicxulub impact crater, Mexico. *Meteoritics & Planetary Science* 39:1069–1088.

Koeberl C., Milkereit B., Overpeck J. T., Scholz C. A., Reimold

W. U., Amoako P. Y. O., Boamah D., Claeys P., Danuor S. K., Deutsch A., Hecky R. E., King J., Newsom H., Peck J., and Schmitt D. 2006. An international and multidisciplinary drilling project into a young complex impact structure: The 2004 ICDP Bosumtwi impact crater, Ghana drilling project—An overview. (abstract #1859). 37th Lunar and Planetary Science Conference. CD-ROM.

Mackenzie G. D., Maguire P. K. H., Denton P., Morgan J. V., and Warner M. 2001. Shallow seismic velocity structure of the Chicxulub impact crater from modelling of Rg dispersion using a genetic algorithm. *Tectonophysics* 338:97–112.

Melosh H. J. 1989. *Impact cratering—A geologic process*. New York: Oxford University Press. 245 p.

Merrill R. B. and Schultz P. H. 1981. *Proceedings of the Conference on Multi-Ring Basins: Formation and Evolution*. New York: Pergamon Press. 289 p.

Milkereit B., Green A., Wu J., White D., and Adams E. 1994. Integrated seismic and borehole geophysical study of the Sudbury igneous complex. *Geophysical Research Letters* 21:931–934.

Morgan J. V., Warner M. R., and the Chicxulub Working Group. 1997. Size and morphology of the Chicxulub impact crater. *Nature* 390:472–476.

Morgan J. V. and Warner M. R. 1999. The third dimension of a multi-ring impact basin. *Geology* 26:407–410.

Morgan J. V., Warner M. R., Collins G. S., Melosh H. J., and Christeson G. L. 2000. Peak-ring formation in large impact craters: Geophysical constraints from Chicxulub. *Earth and Planetary Science Letters* 183:347–354.

Morgan J. V., Warner M., and Grieve R. 2002a. Geophysical constraints on the size and structure of the Chicxulub impact crater. In *Catastrophic events and mass extinctions: Impacts and beyond*, edited by Koeberl C. and MacLeod K. G. GSA Special Paper #356. Boulder, Colorado: Geological Society of America. pp. 49–46.

Morgan J. V., Christeson G. L., and Zelt C. A. 2002b. Testing the resolution tomogram across the Chicxulub crater. *Tectonophysics* 335:215–226.

Naumov M. V. 2002. Impact-generated hydrothermal systems: Data from Popigai, Kara, and Puchezh-Katunki impact structures. In *Impacts in Precambrian shields*, edited by Plado J. and Pesonen L. J. Berlin-Heidelberg: Springer-Verlag. pp. 307–321.

O'Keefe J. D. and Ahrens T. 1999. Complex craters: Relationship of stratigraphy and rings to impact conditions. *Journal of Geophysical Research* 104:27,091–27,104.

O'Keefe J. D., Stewart S. T., Lainhart M. E., and Ahrens T. J. 2001. Damage and rock-volatile mixture effects on impact crater formation. *International Journal of Impact Engineering* 26:543–553.

Ormö J. and Lindström M. 2000. When a cosmic impact strikes the sea bed. *Geological Magazine* 137:67–80.

Pierazzo E., Kring D. A., and Melosh J. H. 1998. Hydrocode simulations of the Chicxulub impact event and the production of climatically active gasses. *Journal of Geophysical Research* 103: 28,607–28,626.

Pierazzo E. and Melosh J. H. 1999. Hydrocode modeling of Chicxulub as an oblique impact event. *Earth & Planetary Science Letters* 165:163–176.

Pilkington M. and Grieve R. A. F. 1992. The geophysical signature of terrestrial impact craters. *Reviews of Geophysics* 30:161–181.

Pilkington M., Hildebrand A., and Ortiz-Aleman C. 1994. Gravity and magnetic field modelling and structure of the Chicxulub crater, Mexico. *Journal Geophysical Research* 99:13,147–13,162.

Pilkington M., Jansa L. F., and Grieve R. A. F. 1995. Geophysical studies of the Montagnais impact crater, Canada. *Meteoritics* 30: 446–450.

Poag C. W. 1996. Structural outer rim of Chesapeake Bay impact crater: Seismic and borehole evidence. *Meteoritics & Planetary Science* 31:218–226.

Poag C. W., Powars D. S., Poppe L. J., and Mixon R. B. 1994. Meteoroid mayhem in the Ole Virginny: Source of the North American tektite strewn field. *Geology* 22:691–694.

Poag C. W., Koeberl C., and Reimold W. U. 2004. *The Chesapeake Bay crater: Geology and geophysics of a late Eocene submarine impact structure*. Berlin-Heidelberg: Springer-Verlag. 522 p.

Popov Y., Romushkevich R., Bayuk I., Korobkov D., Mayr S., Burkhardt H., and Wilhelm H. 2004. Physical properties of the rocks from the upper part of the Yaxcopoil-1 drill hole, Chicxulub crater. *Meteoritics & Planetary Science* 39:799–812.

Powars D. S. and Bruce T. S. 1999. *The effects of the Chesapeake Bay impact crater on the geologic framework and the correlation of hydrogeologic units of southeastern Virginia, south of the James River*. U.S. Geological Survey Professional Paper #1612. Reston, Virginia: U.S. Geological Survey. 82 p.

Schlumberger Educational Services. 1987. *Log interpretation principles/applications*. Houston, Texas: Schlumberger Educational Services. 198 p.

Schlumberger Educational Services. 1989. *Log interpretation principles/applications*. Houston, Texas: Schlumberger Educational Services. 227 p.

Scholz C. A., Karp T., Brooks K. M., Milkereit B., Amoako P. Y. O., and Arko J. A. 2002. Pronounced central uplift identified in the Bosumtwi impact structure, Ghana, using multichannel seismic reflection data. *Geology* 30:939–942.

Schultz P. H. and D'Hondt S. 1996. Cretaceous-Tertiary Chicxulub impact angle and its consequences. *Geology* 24:963–967.

Sclater J. G. and Christie R. A. F. 1980. Continental stretching: An explanation of the post-mid-Cretaceous subsidence of the central North Sea basin. *Journal of Geophysical Research* 85:3711–3739.

Sharpton V. L., Burke K., Camargo-Zanoguera A., Hall S. A., Lee S., Marin L. E., Suarez-R. G., Quezada-M. J. M., Spudis P. D., and Urrutia-Fucugauchi J. 1993. Chicxulub multi-ring impact basin: Size and other characteristics derived from gravity analysis. *Science* 261:1564–1567.

Sharpton V. L., Marin L. E., Carney J. L., Lee S., Ryder G., Schuraytz B. C., Sikora P., and Spudis P. D. 1996. Model of the Chicxulub impact basin. In *The Cretaceous-Tertiary events and other catastrophes in Earth history*, edited by Ryder G., Fastovsky D., and Gartner S. GSA Special Paper #307. Boulder, Colorado: Geological Society of America. pp. 55–74.

Shuvalov V. 2002. Numerical modeling of the impacts into shallow sea. In *Impacts in Precambrian shields*, edited by Plado J. and Pesonen L. J. Berlin-Heidelberg: Springer-Verlag. pp. 323–336.

Shuvalov V., Dypvik H., and Tsikalas F. 2002. Numerical simulations of the Mjølnir marine impact crater. *Journal of Geophysical Research* 107, doi:10.1029/2001JE001968.

Snyder D. B. and Hobbs R. W. 1999a. Deep seismic reflection profiles across the Chicxulub crater. In *Large meteorite impacts and planetary evolution II*, edited by Dressler B. and Sharpton V. L. GSA Special Paper #339. Boulder, Colorado: Geological Society of America. pp. 269–279.

Snyder D. B. and Hobbs R. W. 1999b. *The BIRPS atlas II: A second decade of deep seismic reflection profiling*. London: Geological Society of London. 3 CD-ROMs.

Smelror M., Kelly S. R. A., Dypvik H., Mørk A., Nagy J., and Tsikalas F. 2001. Mjølnir (Barents Sea) meteorite impact ejecta offers a Volgian-Ryazanian boundary marker. *Newsletter on Stratigraphy* 38:129–140.

Stewart S. A. and Allen P. J. 2002. A 20 km diameter multi-ringed impact structure in the North Sea. *Nature* 418:520–523.

Stewart S. A. and Allen P. J. 2005. 3-D seismic reflection mapping of

the Silverpit multi-ringed crater, North Sea. *Geological Society of America Bulletin* 117:354–368.

Sturkell E. and Lindström M. 2004. The target peneplain of the Lockne impact. *Meteoritics & Planetary Science* 39:1721–1731.

Tsikalas F. 1992. A study of seismic velocity, density, and porosity in Barents Sea wells (N. Norway). Master's thesis, University of Oslo, Oslo, Norway. 169 p.

Tsikalas F., Gudlaugsson S. T., and Faleide J. I. 1998a. Collapse, infilling, and post-impact deformation at the Mjølnir impact structure, Barents Sea. *Geological Society of America Bulletin* 110:537–552.

Tsikalas F., Gudlaugsson S. T., and Faleide J. I. 1998b. The anatomy of a buried complex impact structure: The Mjølnir structure, Barents Sea. *Journal of Geophysical Research* 103:30,469–30,484.

Tsikalas F., Gudlaugsson S. T., Eldholm O., and Faleide J. I. 1998c. Integrated geophysical analysis supporting the impact origin of the Mjølnir structure, Barents Sea. *Tectonophysics* 289:257–280.

Tsikalas F., Gudlaugsson S. T., Faleide J. I., and Eldholm O. 1999. Mjølnir structure, Barents Sea: A marine impact crater laboratory. In *Large meteorite impacts and planetary evolution II*, edited by Dressler B. and Sharpton V. L. GSA Special Paper #339. Boulder, Colorado: Geological Society of America. pp. 193–204.

Tsikalas F., Gudlaugsson S. T., Faleide J. I., and Eldholm O. 2002a. The Mjølnir marine impact crater porosity anomaly. *Deep-Sea Research Part II: Topical Studies in Oceanography* 49:1103–1120.

Tsikalas F., Faleide J. I., Eldholm O., and Dypvik H. 2002b. Seismic correlation of the Mjølnir marine impact crater to shallow boreholes. In *Impacts in Precambrian shields*, edited by Plado J. and Pesonen L. J. Berlin: Springer-Verlag. pp. 307–321.

Tsikalas F. and Faleide J. I. 2004. Near-field erosional features at the Mjølnir impact crater: The role of marine sedimentary target. In *Cratering in marine environments and on ice*, edited by Dypvik H., Burchell M., and Claeys Ph. Berlin: Springer-Verlag. pp. 39–55.

Tsikalas F. 2005. Mjølnir crater as a result of oblique impact: Asymmetry evidence constrains impact direction and angle. In *Impact tectonism*, edited by Koeberl C. and Henkel H. Berlin: Springer-Verlag. pp. 285–306.

Ugalde H., Artemieva N., and Milkereit B. 2005. Magnetization on impact structures—Constraints from numerical modelling and petrophysics. In *Large meteorite impacts III*, edited by Kenkmann T., Hörz F., and Deutsch A. GSA Special Paper #384. Boulder, Colorado: Geological Society of America. pp. 25–42.

Ugalde H., Danuor S. K., and Milkereit B. 2007. Integrated 3-D model from gravity and petrophysical data at Lake Bosumtwi impact crater, Ghana. *Meteoritics & Planetary Science* 42:859–866.

Vermeesch P. M. and Morgan J. V. 2004. Chicxulub central crater structure: Initial results from physical property measurements and combined velocity and gravity modelling. *Meteoritics & Planetary Science* 39:1019–1034.

Wyllie M. R. J., Gregory A. R., and Gardner G. H. F. 1956. Elastic wave velocities in heterogeneous and porous media. *Geophysics* 21:41–70.

Wyllie M. R. J., Gregory A. R., and Gardner G. H. F. 1958. An experimental investigation of factors affecting elastic wave velocities in porous media. *Geophysics* 23:459–493.